Attribution of global lake systems change to anthropogenic forcing

Grant, Luke; Vanderkelen, Inne; Gudmundsson, Lukas; Tan, Zeli; Perroud, Marjorie; Stepanenko, Victor M.; Debolskiy, Andrey, V; Droppers, Bram; Janssen, Annette B. G.; Woolway, R. Iestyn; Choulga, Margarita; Balsamo, Gianpaolo; Kirillin, Georgiy; Schewe, Jacob; Zhao, Fang; del Valle, Iliusi Vega; Golub, Malgorzata; Pierson, Don; Marce, Rafael; Seneviratne, Sonia, I; Thiery, Wim

Nature Geoscience

DOI:
10.1038/s41561-021-00833-x

Published: 18/10/2021

Peer reviewed version

Attribution of global lake systems change to anthropogenic forcing

Luke Grant *[1], Inne Vanderkelen[1], Lukas Gudmundsson[2], Zeli Tan[3], Marjorie Perroud[4], Victor M. Stepanenko[5,6], Andrey V. Debolskiy[5,6,7], Bram Droppers[8], Annette B. G. Janssen[8], R. Iestyn Woolway[9], Margarita Choulga[10], Gianpaolo Balsamo[10], Georgiy Kirillin[11], Jacob Schewe[12], Fang Zhao[12], Iliusi Vega del Valle[12], Malgorzata Golub[13], Don Pierson[13], Rafael Marcé[14,15], Sonia I. Seneviratne[2], Wim Thiery[1,2]

[1]Vrije Universiteit Brussel, Department of Hydrology and Hydraulic Engineering, Brussels, Belgium
[2]ETH Zurich, Institute for Atmospheric and Climate Science, Zurich, Switzerland
[3]Pacific Northwest National Laboratory, Richland, WA, USA
[4]University of Geneva, Institute for Environmental Sciences, Geneva, Switzerland
[5]Lomonosov Moscow State University, Moscow, Russia
[6]Moscow Center for Fundamental and Applied Mathematics, Moscow, Russia
[7]Obukhov Institute for Atmospheric Physics, Russian Academy of Science, Moscow, Russia
[8]Wageningen University & Research, Water systems and Global Change, Wageningen, the Netherlands
[9]European Space Agency Climate Office, ECSAT, Harwell Campus, Didcot, Oxfordshire, UK
[10]European Centre for Medium-range Weather Forecasts (ECMWF), Research Department, Reading, UK
[11]Leibniz-Institute of Freshwater Ecology and Inland Fisheries, Berlin, Germany
[12]Potsdam Institute for Climate Impact Research, Potsdam, Germany
[13]Uppsala University, Dept of Ecology and Genetics, Uppsala, Sweden
[14]Catalan Institute for Water Research (ICRA), Girona, Spain
[15]University of Girona, Girona, Spain

Lakes are jeopardized by the impacts of climate change on ice seasonality and water temperatures[1,2]. Yet, historical simulations have not been used to formally attribute observed changes in lake ice and temperature to anthropogenic drivers. Additionally, future projections of these properties are mostly limited to individual lakes or global simulations from single lake models[3,4]. Here we uncover the human imprint on lakes worldwide using novel hindcasts[5] and projections from

*corresponding author, email: luke.grant@vub.be

five lake models. Reconstructed trends in lake temperature and ice cover in recent decades are extremely unlikely to be explained by pre-industrial climate variability alone and ice cover trends are consistent with lake model simulations under historical conditions, providing the first formal attribution of lake changes to anthropogenic climate change. Moreover, lake temperature, ice thickness, and ice cover scale robustly with air temperature across future climate scenarios. Importantly, the uncertainty in end-of-century impacts is dominated by the choice of emissions scenario rather than lake model or forcing types, showing that lake systems will greatly benefit from climate mitigation. Otherwise, these impacts would profoundly alter the functioning of worldwide lake ecosystems and the services they provide.

Lakes provide ecosystem services to local communities[6,7] and modulate local climates[8–12]. The seasonality of lake ice cover and lake temperatures are the foundations of the lake environment, controlling many lake processes[13,14]. In recent decades, lake temperatures have been rising and seasonal ice cover has been declining on regional[15–17] and global scales[1–3]. Among other things, these changes alter lake stratification, impact lake ecosystem productivity[18] and disturb fisheries[19,20].

New historical reconstructions of lake ice cover and mixed-layer temperature from the ERA5-Land reanalysis[5] provide a high-resolution outlook on these changes in recent decades (Fig. 1a-c, Supplementary Fig. 1). From 1981-1990 until 2010-2019, these reconstructions reveal rapid changes; 130,472 lake grid cells worldwide have experienced two weeks of lake ice cover loss, while on average lakes have lost 9 days of ice cover. Likewise, global-scale reconstructed lake mixed layer temperature shows substantial increases, with 64,382 lake grid cells warming more than 1.5 °C and a global annual average increase of 0.4 °C (Fig. 2e).

While observed and reconstructed changes in lake ice cover and lake temperatures are large, the possibility that they are due to natural climate variability has so far not been ruled out. They have also not been attributed to anthropogenic drivers using formal statistical approaches. Formally, "detection"[21,22] of climate change impacts consists of showing that observed changes are inconsistent with natural variability by comparing them against simulated variability under human-free climate conditions. Upon successful detection, anthropogenic greenhouse gas emissions are a plausible candidate to explain ongoing changes in lakes, but this causal link must again be formally established. Such "Attribution"[21,22] to anthropogenic emissions is achieved by showing consistencies between observed changes and response patterns derived from historical climate impact simulations. Together, detection and attribution represent a cornerstone of assessments by the Intergovernmental Panel on Climate Change (IPCC)[23,24].

Climate change detection and attribution We investigate climate change detection and attribution in ERA5-Land reconstructed lake variables using two complementary approaches

and novel simulations with five global-scale lake models forced by four global climate models (GCMs)[25] (see Methods and Supplementary Note 1). The first approach[26–28] considers a distribution of rank correlations between the multi-model mean of lake simulations forced by GCMs under historical climate forcings (HIST) and a collection of individual pre-industrial control (PIC) lake simulations. This distribution of correlations, assumed to arise from pre-industrial climate variability, is compared to the single correlation between HIST and the reconstructed time series (OBS for "observations"). Here, detection is inferred by rejecting the null-hypothesis that reconstructed trends are consistent with the distribution of correlations representative of pre-industrial climate variability (correlation-based approach[29]; Fig. 2a-d). The second approach employs Regularised Optimal Fingerprinting[21,30]. Here, the slope parameters (henceforth referred to as scaling factors) that scale HIST to fit OBS in a total least-squares regression communicate detection when they are significantly different from 0 (that is, when the 95% confidence intervals of the scaling factors exclude 0). Attribution is achieved when scaling factors additionally overlap with unity.

Strict attribution to anthropogenic emissions requires both all-forcings historical and natural historical response patterns (including for instance solar and volcanic influences but without anthropogenic emissions). Our experimental framework includes a pre-industrial control instead of a natural historical climate scenario and therefore limits formal attribution to all combined historical forcings (see Methods). However, in light of the dominant role of anthropogenic emissions relative to natural forcings in historical climate change[31], we argue that any attribution in this framework entails the imprint of human influence.

For lake water temperature at 2 m depth (hereafter lake temperature), the correlation-based approach shows a strong distinction between the correlation of OBS and HIST and the distribution of correlation coefficients of HIST and PIC (Fig. 2a). This implies that lake temperature reconstructions for the recent past lie outside the typical variability of pre-industrial climate and therefore cannot be explained by pre-industrial climate variability (>99% confidence level). For ice onset, break-up, and duration, correlations between OBS and HIST anomalies are again substantially larger than HIST versus PIC correlations (Fig. 2b-d) and also significant (at a confidence level of 95%, 95%, and 99%, respectively). Overall this supports the detection of a climate change signal in lake temperature and all three lake ice indices.

Scaling factor confidence intervals for lake temperature and all three ice indices are significantly different from 0, confirming the detection of a climate change imprint in all four variables (Fig. 2e-h). For ice onset, break-up and duration, the HIST time series closely resembles OBS, and scaling factors overlap with unity (Fig. 2g-h), providing strong evidence to attribute changes in these variables to external forcings. On the whole, this formal statistical evidence confirms that external forcings - and by extension, anthropogenic emissions - can explain reconstructed changes in lake ice onset, break-up and duration.

Future climate projections Only a few recent studies[1,3,4] project end-of-century changes in lake temperature and ice cover over large areas under multiple GCM forcings and representative concentration pathways (RCPs), thereby accounting for uncertainties related to meteorological forcing and climate scenario. However, these studies so far disregard both lake model uncertainty and transient lake response to greenhouse gas forcing. Having demonstrated the foregone imprint of climate change on lakes, we project lake temperature and ice conditions across pre-industrial to future periods (1661-2099) under RCPs 2.6, 6.0 and 8.5 (see Methods).

By the end of the century, annual mean lake temperatures increase and ice cover decreases unanimously under the high-emission scenario RCP 8.5 (Fig. 3a-e). Lakes warm the most (+4-5 °C by 2070-2099 relative to 1971-2000) in southern temperate latitudes in North America and in temperate latitudes across Eurasia (Fig. 3a, Supplementary Fig. 2-7). In many boreal zones, the June-July-August lake temperature warming exceeds global mean surface air temperature warming by a factor of 1.5-2 (Fig. 3b), indicating a high climate sensitivity for these lakes associated with the polar amplification of atmospheric warming. These spatial sensitivity patterns are consistent across RCPs for lake temperature (Supplementary Fig. 8-10), ice thickness (Supplementary Fig. 11-13) and ice cover indices (Supplementary Fig. 14-16). Ice duration decreases by 28-80 days (5^{th} to 95^{th} percentile), with the largest reductions occurring in coastal regions and Scandinavia ($>$ 45 days, Fig. 3e). Ice duration projections are mostly driven by changes in the timing of ice break-up, which happens consistently earlier in the year by the end of the century and agrees with the seasonality of ice thickness losses (Fig. 3c-e, See Supplementary Fig. 17-22).

In all future scenarios, global mean lake temperatures increase while ice thickness and ice duration decrease (Fig. 4). Multi-model mean projections under RCPs 2.6, 6.0 and 8.5 diverge by 2050 at the latest, with only RCP 2.6 showing an end-of-century stabilization (Fig. 4a-c). Global mean projections show high inter-model consistency for all variables, except for ice thickness computed by Community Land Model version 4.5 (See Supplementary Fig. 23-25). By 2100, the scenario spread exceeds the uncertainty originating from the lake models, GCMs and natural variability, underscoring the value of mitigation for avoiding severe lake system changes.

Across all future climate scenarios, multi-model mean lake temperature, ice thickness and ice cover scale robustly with air temperature at the global mean level. Projected average global annual mean scaling for lake temperature, ice duration and ice thickness are +0.9 °C/°C_{air}, -9.7 days/°C_{air} and -0.033 m/°C_{air}, respectively. RCP 8.5 projections indicate end-of-century global mean anomalies of +4.0 °C for lake temperature, -0.17 m for ice thickness and a 46 decrease in days for ice duration.

Discussion Our projections reveal coastal-inland gradients in ice duration projections around northern European and Scandinavian coasts and far eastern and western North America that agree with previous studies[32]. Large decreases in ice thickness projected in spring months relative to fall months (Supplementary Fig. 17-19) agree with observed changes in lake ice cover

around the northern hemisphere[16,33,34]. This is also consistent with the dominant contribution of earlier ice break-up dates to ice duration changes relative to delayed ice onset (Supplementary Fig. 14-16,20-22), which has been ascribed to a stronger climate change impact on the spring return of the 0°C isotherm than its fall timing[35]. At the global mean level, our lake temperature and ice cover projections for 2100 (Supplementary Fig. 23,25) agree with RCP 2.6 and 6.0 projections from a single lake model study over a smaller set of lakes[3].

Challenges to global scale lake modelling arise from parameter value selection, the spatiotemporal coverage and quality of reference products and the selection of adequate impact variables. While anchored to reality through the step-wise bias-correction of their boundary conditions[5] (see Methods), the lake variables of ERA5-Land are diagnostics and not subject to direct assimilation with remote sensing or in-situ data. Furthermore, ERA5-Land provides only mixed layer temperature, which we assume to correspond to 2 m depth to enable comparison with the lake models. While a discrepancy between the global average mixed layer depth of the reconstructions and the lake model 2 m depth could invalidate this assumption, it also provides a candidate physical explanation for the positive lake temperature biases precluding attribution of this variable (Supplementary Fig. 26, Fig. 4). Despite these limitations, ERA5-Land is the only available reference product with sufficient spatial and temporal extent to be suitable for detection and attribution purposes. Moreover, a comparison of lake surface temperatures for 272 lakes across the globe shows strong agreement between the reconstruction and in situ/remote sensing data (Supplementary Fig. 29), corroborating earlier evaluation efforts and confirming that ERA5-Land can be used as a reference in our study (Supplementary Note 1). Furthermore, the lake model skill (Supplementary Fig. 27,28, Supplementary Note 2) and inter-model agreement both at the global scale (Supplementary Fig. 23-25) and with respect to latitudinal, coastal and seasonal characteristics (Supplementary Fig. 2-22) adds confidence to the quality of our projections. Future attribution studies may, however, benefit from the ongoing development of global-scale, multi-decade lake temperature and ice cover data sets based on remote sensing[36]. As reference data sets and lake models update in the near future, optimal fingerprinting techniques may provide even more robust arguments for detection and attribution.

In summary, we showed increases in lake temperature and decreases in ice cover with strong inter-model consistency using an ensemble of five global-scale lake models. We demonstrate that reconstructed historical changes in lakes worldwide are *extremely unlikely* to have occurred due to pre-industrial climate variability alone and attribute their changes in ice cover indices to anthropogenic emissions. Our ensemble framework encompasses climate model, lake model, natural variability and scenario uncertainties, which bolsters our projections and reduces sampling uncertainties in detecting and attributing the anthropogenic signal in historical lake variable changes. These projected changes could have manifold consequences for lake thermal regimes, lake ecological processes and provision of lake ecosystem services. The clear dependency of our projections on the radiative forcing scenario and the strong arguments we make for

reconstructed changes being both unexplainable by pre-industrial climate variability alone and consistent with anthropogenic forcings underline the benefit of stabilizing lake systems through major societal adjustments towards mitigating climate change.

Methods

ISIMIP We perform global-scale simulations with five lake models as a part of phase 2b of the Inter-Sectoral Impact Model Intercomparison Project (ISIMIP2b). All simulations adhere to the lake sector protocol (`https://www.isimip.org/protocol/#isimip2b`), which determines simulated periods and scenarios, lake model forcing datasets, the spatial and temporal resolutions of model outputs and lake locations and depths. Pre-industrial control simulations (1661-2099) assume a pre-industrial climate without anthropogenic greenhouse gas forcing[25]. Historical simulations (1861-2005) use a historical climate, whereas future projections (2006-2099) consider RCPs 2.6, 6.0 and 8.5. Four GCMs contributing to phase 5 of the Coupled Model Intercomparison Project (CMIP5) - GFDL-ESM2M, HadGEM2-ES, IPSL-CM5A-LR and MIROC5 - are used as input to the lake models after bias-adjustment to the EWEMBI reference dataset[25,37].

The lake models contributing to this study are the Community Land Model version 4.5 (CLM4.5)[38], the Arctic Lake Biogeochemistry Model (ALBM)[39], SIMSTRAT-UoG[40], VIC-lake[41] and LAKE[42]. All lake models operate globally at $0.5^\circ \times 0.5^\circ$ horizontal resolution. Since most real lakes are sub-grid features at this spatial resolution, simulated lake pixels are termed representative lakes in their location. Depth and summed grid-scale area fraction represent those of real lakes contained within the ISIMIP grid cells. Locations and grid-scale fractions of real lakes are determined by the Global Lakes and Wetlands Database (GLWD)[43]. All models but CLM4.5 use a $0.5^\circ \times 0.5^\circ$ lake depth field aggregated from the original 30 arc sec Global Lake Data Base (GLDB)[44–46]. CLM4.5 lakes are computed with 51-meter depths in each lake containing grid cell. Model characteristics are provided in Supplementary Table 1.

ERA5-Land We use ERA5-Land reanalysis lake ice depth and mixed layer temperature reconstructions as reference for lake model evaluation and climate change detection and attribution[5]. The ERA5-Land product delivers lake variables at 0.1° horizontal and hourly temporal resolution computed by the Fresh-water Lake model (FLake). ERA5-Land is a land-only re-run of ERA5 with a finer resolution for improved application as reference product for land-based energy and water flux studies. The ERA5-Land reanalysis uses lower atmospheric forcing from the ERA5 reanalysis as boundary conditions and is therefore bounded by observations through their assimilation in ERA5. Lake model computations are embedded as a tile in the Tiled ECMWF Scheme for Surface Exchanges over Land incorporating land surface hydrology (HTESSEL)[47]. Here, lake variables are computed in each grid cell where inland water bodies cover at least 1% of the surface area of the cell. At the time of analysis, this dataset spans 1981 to 2019 (inclusive).

Data processing Post-processing of model ice thickness outputs was performed to attain homogenized ice onset, break-up and duration values. Ice cover indices were calculated with hydrological years, defined as year-long periods which contain ice onset or break-up dates for

lakes in the northern hemisphere. For ice onset calculations, we select the October to September hydrological year and convert each pixel value with ice cover to the day of the year of its time step. After this, we added 365 to periods between 1st January and 30th September so that the days of the year monotonically increase during one hydrological year. A temporal minimum was calculated across this adjusted October 1st (year t), to September 30th, (year t+1 series). This was performed for all available October to September hydrological years in the series, resulting in annual maps of ice start dates. The same process with a temporal maximum calculation across its September to August hydrological year was done for ice break-up calculations, resulting in maps of annual ice end dates. Ice duration is computed as the sum of all "ice-on" days across the October to September hydrological year. We analyze lake temperature at 2 m depth to enable comparison against ERA5-Land mixed layer temperatures and to avoid an overly strong dependence on surface air temperature which can be expected from lake surface temperatures analyses. Global mean calculations on ice thickness datasets include all pixels without ice cover. Reanalysis data are coarsened to the $0.5° \times 0.5°$ ISIMIP grid. Before calculating spatial means, all data sets are masked for overlapping pixels between lake model simulations and reanalysis data.

Detection and Attribution We generate all-forcings response patterns (HIST) by concatenating each ISIMIP lake model's historical time series (1861-2005) with the RCP 8.5 (2006-2099) future simulations to sample forced response patterns for the same period as the ERA5-Land reconstructions (1981-2019; OBS). Next, global annual means are computed from these series, yielding a total of 40 HIST realizations (8 per lake model). For a forced response pattern without human influence (PIC), all available ISIMIP pre-industrial control simulations are concatenated for each lake model and cut into non-overlapping global mean "chunks" matching the time span of the reconstructions. This ideally provides 44 (11×4) chunks of pre-industrial climate variability driven simulations per lake model if pre-industrial control simulations span 1661-2099 for each GCM forcing. While some lake models have only computed pre-industrial simulations Reconstructions and response patterns are then computed as anomalies through temporal centering (each series is subtracted by its temporal mean) and applied to two detection and attribution approaches; a correlation-based view on detection and Regularised Optimal Fingerprinting (ROF) to confirm detection and attribution.

The correlation approach (Figure 2a-d), uses all available HIST and PIC anomalies without smoothing. For each lake variable, Spearman (rank) correlation coefficients are calculated between the global annual mean of all available historical simulations (HIST) and every available global annual mean PIC chunk. These correlation coefficients comprise the empirical distributions in Figure 2. A correlation coefficient is then computed between OBS and the mean of the HIST ensemble, plotted as a red vertical line. A normal distribution ($Z \sim N(mean(corr(PIC, HIST)), std(corr(PIC, HIST)))$) is assumed for reporting the 95% and 99% confidence levels for comparison with OBS-HIST correlation. We use the Spearman correlation coefficient because of its resistance to outliers, however, results are consistent with

a Pearson correlation.

We use Regularised Optimal Fingerprinting (ROF) with a Total Least-Squares (TLS) regression to compute scaling factors which fit annual mean HIST anomalies (here only the RCP 8.5 versions to avoid artificial consistencies among historical, 1981-2005 sections of anomalies) to reconstructions (OBS) at the global mean level (Figure 2e-h). This follows a generalised linear regression model of the form:

$$\mathbf{y} = \mathbf{X}\boldsymbol{\beta} + \varepsilon$$

where $\mathbf{y}$ is a vector of n observations (ERA5-Land lake reconstructions; OBS), $\mathbf{X}$ is a matrix of m columns of multi-model mean simulated response patterns (ISIMIP simulations), $\boldsymbol{\beta}$ is a vector of scaling factors and ε is the regression residual, representing the internal variability in $\mathbf{y}$. We take a single-factor approach; the regression fit is performed for one response pattern at a time (HIST) and therefore $\mathbf{X}$ only contains one column or response pattern (m = 1). In a TLS framework, the regression is computed to minimize residuals perpendicular to the best fit line[22]. This addresses uncertainty in $\mathbf{X}$, underlining the assumption in TLS that response patterns are not perfectly known. TLS is, therefore, a strong choice for small ensemble study-cases with greater sampling uncertainty, contrasting the Ordinary Least-Squares approach wherein fitting by minimizing vertical residuals assumes the response patterns in $\mathbf{X}$ are perfectly known. The TLS regression is achieved through a singular value decomposition (SVD) on $[\mathbf{y}, \mathbf{X}]$.

Before the TLS fit, observations and response patterns are converted to 5-year block means, temporally centered (subtracted by their mean) and pre-whitened. Pre-whitening to achieve unit noise is the "optimization" of signals in ROF. This is done with a regularised covariance matrix, $\widehat{\boldsymbol{C}}_1$, which represents internal variability in our lake variables. $\widehat{\boldsymbol{C}}_1$ is derived from one of two covariance estimates, $\boldsymbol{C}_1$ and $\boldsymbol{C}_2$, computed from equal-sized samples of available PIC chunks. Key to ROF, regularisation involves conforming $\widehat{\boldsymbol{C}}_1$ to equal $\lambda\boldsymbol{C}_1 + \rho\boldsymbol{I}$. Here, $\mathbf{I}$ is the identity matrix, and λ and ρ are coefficients whose estimators are provided by Ledoit and Wolf[48]. This avoids underestimating the lowest eigenvalues of $\widehat{\boldsymbol{C}}_1$, which translates to a conservative estimate of noise[30]. $\boldsymbol{C}_2$ is used for calculating the confidence intervals on scaling factors and performing a residual consistency test (RCT). Final computations of scaling factors, their confidence intervals and RCTs are taken as the median of 1000 realizations of ROF through shuffling the PIC chunks from which $\boldsymbol{C}_1$ and $\boldsymbol{C}_2$ are computed[28].

The RCT validates the residuals in the TLS regression against the assumed internal variability[30]. Here, $\boldsymbol{C}_2$ and $\mathbf{X}$ are used in Monte Carlo simulations to bootstrap 1000 samples of virtual observations, fingerprints and covariance matrices assuming a perfect fit with $\boldsymbol{\beta} = 1$. The smallest squared singular value (or eigenvalue, λ) of the SVD in the original TLS fit - representing the residuals in the regression - is then corrected and used as a test statistic against 1000 virtual eigenvalues ($\lambda_{\text{virt,i=1,...1000}}$) and their kernel density estimates (i.e λ is tested against 1000

virtual, empirical distributions). The RCT is passed if λ is consistent with these distributions, which is considered true if the average position of λ in the virtual distributions yields a p-value greater than 0.10 (see Supplementary Note 3).

Future projections We calculate all maps as signals across 1971-2000 and 2070-2099 mean baseline and future periods. For scaling, each signal map is first divided by the change in global mean air temperature for the same period before calculating ensemble means. For each GCM-Lake model combination, we compute global mean anomalies relative to the global temporal average of the pre-industrial control simulation (Fig. 4). Global mean air temperature series from GCMs are treated the same. In panels d, e and f of figure 4, series are smoothed with a 21-year running mean to reduce natural variability effects.

Data Availability The ISIMIP2b lake sector simulations presented in this study are available through the Earth System Grid Federation (ESGF, `https://esgf-data.dkrz.de/`). The ERA5-Land lake data used in this study are developed by the European Centre for Medium-Range Weather Forecasts (ECMWF) and are available through the Copernicus Climate Change Service's Climate Data Store (CDS, `https://cds.climate.copernicus.eu/cdsapp#!/search?type=dataset`). The observed lake surface temperatures used for validating ERA5-Land can be found here `https://portal.lternet.edu/nis/mapbrowse?packageid=knb-lter-ntl.10001.3`.

Code Availability All codes used to generate the analyses are available through the github repository of the Department of Hydrology and Hydraulic Engineering at VUB (`https://github.com/VUB-HYDR/2020_Grant_etal`).

References

[1] Sharma, S. *et al.* Widespread loss of lake ice around the Northern Hemisphere in a warming world. *Nat. Clim. Chang.* **9**, 227–231 (2019).

[2] O'Reilly, C. M. *et al.* Rapid and highly variable warming of lake surface waters around the globe. *Geophys. Res. Lett.* 1–9 (2015).

[3] Woolway, R. I. & Merchant, C. J. Worldwide alteration of lake mixing regimes in response to climate change. *Nat. Geosci.* **12**, 271–276 (2019).

[4] Maberly, S. C. *et al.* Global lake thermal regions shift under climate change. *Nat. Commun.* **11**, 1–9 (2020).

[5] Copernicus Climate Change Service (C3S): C3S ERA5-Land reanalysis. CDS https://cds.climate.copernicus.eu/cdsapp#!/home (2019) .

[6] Mueller, H., Hamilton, D. P. & Doole, G. J. Evaluating services and damage costs of degradation of a major lake ecosystem. *Ecosyst. Serv.* **22**, 370–380 (2016).

[7] Rinke, K., Keller, P. S., Kong, X., Borchardt, D., & Weitere, M. *Atlas of Ecosystem Services Ch. 3: Ecosystem Services from Inland Waters and Their Aquatic Ecosystems* (Springer, Cham, 2019).

[8] Bonan, G. Sensitivity of a GCM Simulation to Inclusion of Inland Water Surfaces. *J. Clim.* **8**, 2691–2704 (1995).

[9] Subin, Z. M., Murphy, L. N., Li, F., Bonfils, C. & Riley, W. J. Boreal lakes moderate seasonal and diurnal temperature variation and perturb atmospheric circulation: Analyses in the Community Earth System Model 1 (CESM1). *Tellus, Ser. A Dyn. Meteorol. Oceanogr.* **64** (2012).

[10] Thiery, W. *et al.* LakeMIP Kivu: Evaluating the representation of a large, deep tropical lake by a set of one-dimensional lake models. *Tellus, Ser. A Dyn. Meteorol. Oceanogr.* **66**, 1–18 (2014).

[11] Thiery, W. *et al.* The impact of the African Great Lakes on the regional climate. *J. Clim.* **28**, 4061–4085 (2015).

[12] Scott, R. W. & Huff, F. A. Impacts of the Great Lakes on regional climate conditions. *J. Great Lakes Res.* **22**, 845–863 (1996).

[13] Griffiths, K., Michelutti, N., Sugar, M., Douglas, M. S. & Smol, J. P. Ice-cover is the principal driver of ecological change in High Arctic lakes and ponds. *PLoS One* **12** (2017).

[14] Tan, Z., Yao, H. & Zhuang, Q. A Small Temperate Lake in the 21st Century: Dynamics of Water Temperature, Ice Phenology, Dissolved Oxygen, and Chlorophyll a. *Water Resour. Res.* **54**, 4681–4699 (2018).

[15] Austin, J. A. & Colman, S. M. Lake Superior summer water temperatures are increasing more rapidly than regional temperatures: A positive ice-albedo feedback. *Geophys. Res. Lett.* **34**, 1–5 (2007).

[16] Ghanbari, R. N., Bravo, H. R., Magnuson, J. J., Hyzer, W. G. & Benson, B. J. Coherence between lake ice cover, local climate and teleconnections (Lake Mendota, Wisconsin). *J. Hydrol.* **374**, 282–293 (2009).

[17] Duguay, C. R. *et al.* Recent trends in Canadian lake ice cover. *Hydrol. Process.* **20**, 781–801 (2006).

[18] O'Reilly, C., Alin, S., Piisnier, P.-D., Cohen, A. & McKee, B. Climate change decreases aquatic ecosystem productivity of Lake Tanganyika, Africa. *Nature* **424**, 766–768 (2003).

[19] Hansen, G. J., Read, J. S., Hansen, J. F. & Winslow, L. A. Projected shifts in fish species dominance in Wisconsin lakes under climate change. *Glob. Chang. Biol.* **23**, 1463–1476 (2017).

[20] Lyons, J. *et al.* Trends in the reproductive phenology of two great lakes fishes. *Trans. Am. Fish. Soc.* **144**, 1263–1274 (2015).

[21] Ribes, A., Azaís, J. M. & Planton, S. Adaptation of the optimal fingerprint method for climate change detection using a well-conditioned covariance matrix estimate. *Clim. Dyn.* **33**, 707–722 (2009).

[22] Allen, M. R. & Stott, P. a. Estimating signal amplitudes in optimal fingerprinting, part I: Theory. *Clim. Dyn.* **21**, 477–491 (2003).

[23] Bindoff, N. L. *et al.* Detection and attribution of climate change: From global to regional. In *Clim. Chang. 2013 Phys. Sci. Basis Work. Gr. I Contrib. to Fifth Assess. Rep. Intergov. Panel Clim. Chang.*, 867–952 (Cambridge University Press, Cambridge, 2013).

[24] Gillett, N. P. *et al.* The Detection and Attribution Model Intercomparison Project. *Geosci. Model Dev.* **9**, 3685–3697 (2016).

[25] Frieler, K. *et al.* Assessing the impacts of global warming - Simulation protocol of the Inter-Sectoral Impact Model Intercomparison Project (ISIMIP2b). *Geosci. Model Dev.* **10**, 4321–4345 (2017).

[26] Wan, H., Zhang, X., Zwiers, F. & Min, S. K. Attributing northern high-latitude precipitation change over the period 1966–2005 to human influence. *Clim. Dyn.* **45**, 1713–1726 (2015).

[27] Qian, C. & Zhang, X. Human influences on changes in the temperature seasonality in mid- to high-latitude land areas. *J. Clim.* **28**, 5908–5921 (2015).

[28] Gudmundsson, L., Seneviratne, S. I. & Zhang, X. Anthropogenic climate change detected in European renewable freshwater resources. *Nat. Clim. Chang.* **7**, 813–816 (2017).

[29] Padron, R. *et al.* Observed changes in dry season water availability attributed to human-induced climate change (accepted). *Nat. Geosci.* (2020).

[30] Ribes, A., Planton, S. & Terray, L. Application of regularised optimal fingerprinting to attribution. Part I: Method, properties and idealised analysis. *Clim. Dyn.* **41**, 2817–2836 (2013).

[31] Myhre, G. *et al.* Anthropogenic and natural radiative forcing. In *Clim. Chang. 2013 Phys. Sci. Basis Work. Gr. I Contrib. to Fifth Assess. Rep. Intergov. Panel Clim. Chang.*, 659–740 (Cambridge University Press, Cambridge, 2013).

[32] Dibike, Y., Prowse, T., Saloranta, T. & Ahmed, R. Response of Northern Hemisphere lake-ice cover and lake-water thermal structure patterns to a changing climate. *Hydrol. Process.* **25**, 2942–2953 (2011).

[33] Bonsal, B. R., Prowse, T. D., Duguay, C. R. & Lacroix, M. P. Impacts of large-scale teleconnections on freshwater-ice break/freeze-up dates over Canada. Journal of Hydrology, 330: 340-353. *J. Hydrol.* **330**, 340–353 (2006).

[34] Korhonen, J. Long-term changes in lake ice cover in Finland. *Water Policy* **37**, 347–363 (2006).

[35] Bonsal, B. R. & Prowse, T. D. Trends and variability in spring and autumn °C-isotherm dates over Canada. *Clim. Change* **57**, 341–358 (2003).

[36] Giardino, C., Merchant, C. & Simis, S. Preparing for the first Lakes ECV climate data record. *ESA Clim. Chang. Initiat. - Lakes Newsl.* (2019).

[37] Lange, S. EartH2Observe, WFDEI and ERA-Interim data Merged and Bias-corrected for ISIMIP (EWEMBI). V.1.1. GFZ Data Services. http://doi.org/10.5880/pik.2019.004. Accessed 18-04-2019. (2019).

[38] Lawrence, D. M. *et al.* Parameterization improvements and functional and structural advances in Version 4 of the Community Land Model. *J. Adv. Model. Earth Syst.* **3**, 1–27 (2011).

[39] Tan, Z., Zhuang, Q. & Anthony, K. W. Modeling methane emissions from arctic lakes: Model development and site-level study. *J. Adv. Model. Earth Syst.* **7**, 459–483 (2015).

[40] Goudsmit, G.-H. Application of $\kappa - \varepsilon$ turbulence models to enclosed basins: The role of internal seiches. *J. Geophys. Res.* **107**, 3230–3243 (2002).

[41] Bowling, L. C. & Lettenmaier, D. P. Modeling the effects of lakes and wetlands on the water balance of arctic environments. *J. Hydrometeorol.* **11**, 276–295 (2010).

[42] Stepanenko, V. *et al.* LAKE 2.0 : a model for temperature , methane , carbon dioxide and oxygen dynamics in lakes. *Geosci. Model Dev.* **9**, 1977–2006 (2016).

[43] Lehner, B. & Döll, P. Development and validation of a global database of lakes, reservoirs and wetlands. *J. Hydrol.* **296**, 1–22 (2004).

[44] Kourzeneva, E., Asensio, H., Martin, E. & Faroux, S. Global gridded dataset of lake coverage and lake depth for use in numerical weather prediction and climate modelling. *Tellus, Ser. A Dyn. Meteorol. Oceanogr.* **64** (2012).

[45] Subin, Z. M., Riley, W. J. & Mironov, D. An improved lake model for climate simulations: Model structure, evaluation, and sensitivity analyses in CESM1. *J. Adv. Model. Earth Syst.* **4**, 1–27 (2012).

[46] Choulga, M., Kourzeneva, E., Zakharova, E. & Doganovsky, A. Estimation of the mean depth of boreal lakes for use in numerical weather prediction and climate modelling. *Tellus, Ser. A Dyn. Meteorol. Oceanogr.* **66** (2014).

[47] Balsamo, G. *et al.* Evolution of land surface processes in the IFS. *ECMWF Newsl.* **127**, 17–22 (2011).

[48] Ledoit, O. & Wolf, M. A well-conditioned estimator for large-dimensional covariance matrices. *J. Multivar. Anal.* **88**, 365–411 (2004).

Acknowledgements We are grateful to the Potsdam Institute for Climate Impact Research (PIK) for initiating and coordinating the ISIMIP initiative, with special thanks to Matthias Büchner for his oversight of ISIMIP data publishing, and to the modelling centres for making their impact simulations publicly available through ESGF. We owe many thanks to Friederike Fröb and Alexander Winkler for sharing their Regularised Optimal Fingerprinting python code, and to Martin Schmid for the helpful discussions. We also thank the National Center for Atmospheric Research (NCAR) for maintaining CLM and making the source code publicly available. I.V. is a research fellow at the Research Foundation Flanders (FWO) (FWOTM920). W.T. acknowledges the Uniscientia Foundation and the ETH Zurich Foundation for their support to this research. Z.T. is supported by the U.S. DOE's Earth System Modeling program through the Energy Exascale Earth System Model (E3SM) project. The computational resources and services used in this work were provided by the VSC (Flemish Supercomputer Center), funded by the Research Foundation - Flanders (FWO) and the Flemish Government – department EWI. R.M participated trough the project WATExR of the JPI Climate ERA4CS Program, and acknowledges funding from the CERCA program of the Generalitat de Catalunya. V.M.S. and A.V.D. used the resources of Moscow State University Supercomputer Center ("Lomonosov-2" supercomputer).

Author Contributions L.Gr., I.V. and W.T. designed the study. L.Gr. wrote the manuscript with support from all authors and performed all analyses under the supervision of I.V. and W.T.. L.Gu. provided guidance on the detection analysis. Z.T., M.P., V.M.S., A.V.D., B.D., A.B.G.J., S.I.S. and W.T. conducted the global lake model simulations. J.S., F.Z., M.G., D.P., R.M. and W.T. coordinated the ISIMIP lake sector activities.

Author Information The authors declare no Competing Interests.

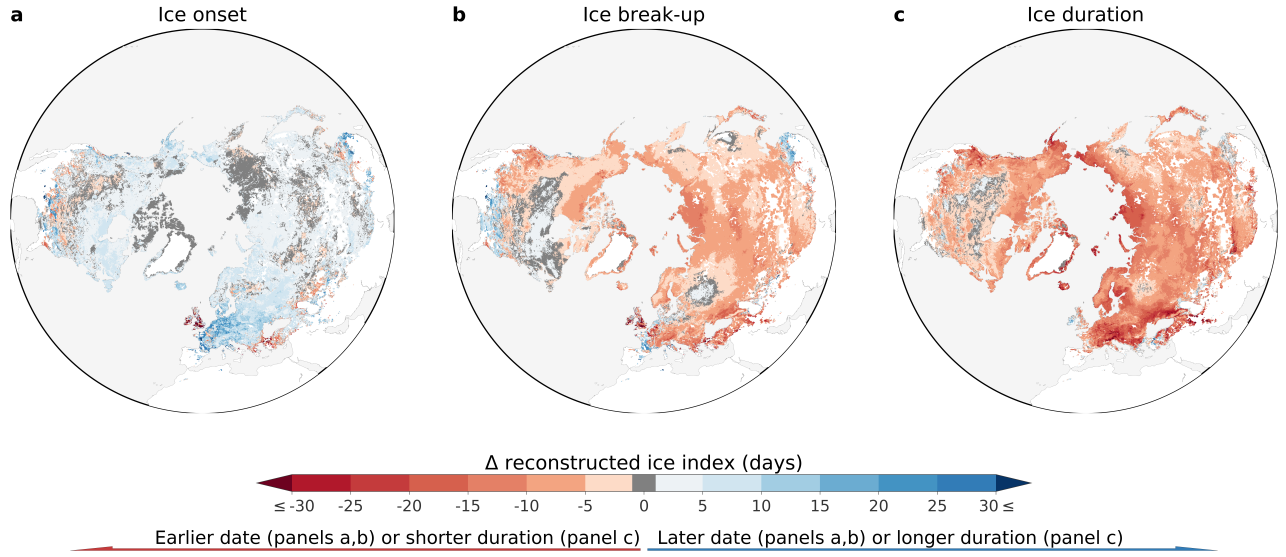

Figure 1: **Reconstructed historical lake ice changes.** Changes in ice onset (**a**), ice break-up (**b**) and ice duration (**c**) in 40 years across baseline (1981-1990) and recent (2010-2019) periods as obtained from ERA5-Land.

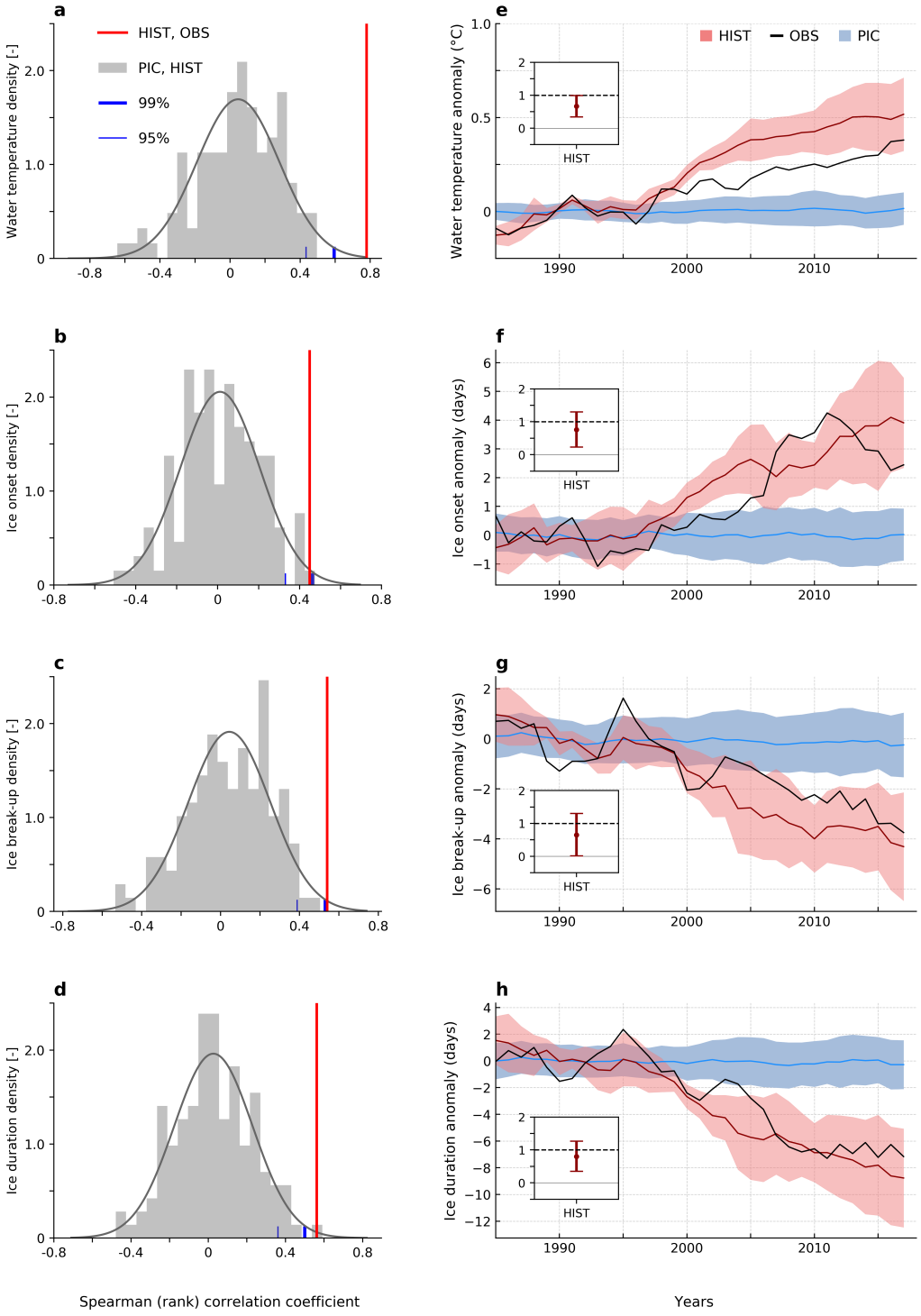

Figure 2: **Detection and attribution of the human imprint on lake variables.** Empirical distribution of Spearman correlation coefficients between all available PIC chunks (realizations of pre-industrial climate variability selected across 1661-2099) and the HIST response pattern (the multi-model mean historical realization) for lake temperature (**a**), ice onset (**b**), ice break-up (**c**) and ice duration (**d**). Red lines show the correlation coefficient between the HIST series and OBS (ERA5-Land reconstructions). Vertical blue lines mark the 95% and 99% cumulative probability of an assumed normal distribution for the sample of PIC-HIST coefficients. Global multi-model mean time series for HIST and PIC forced response patterns and OBS smoothed by a 5-year running mean for lake temperature (**e**), ice onset (**f**), ice break-up (**g**) and ice duration (**h**). Results of single-factor ROF output on HIST are displayed in insets. Here, scaling factor confidence intervals denote their 0.5-99.5% uncertainty range and infer detection when excluding the 0 line. Attribution is achieved when confidence intervals additionally include unity.

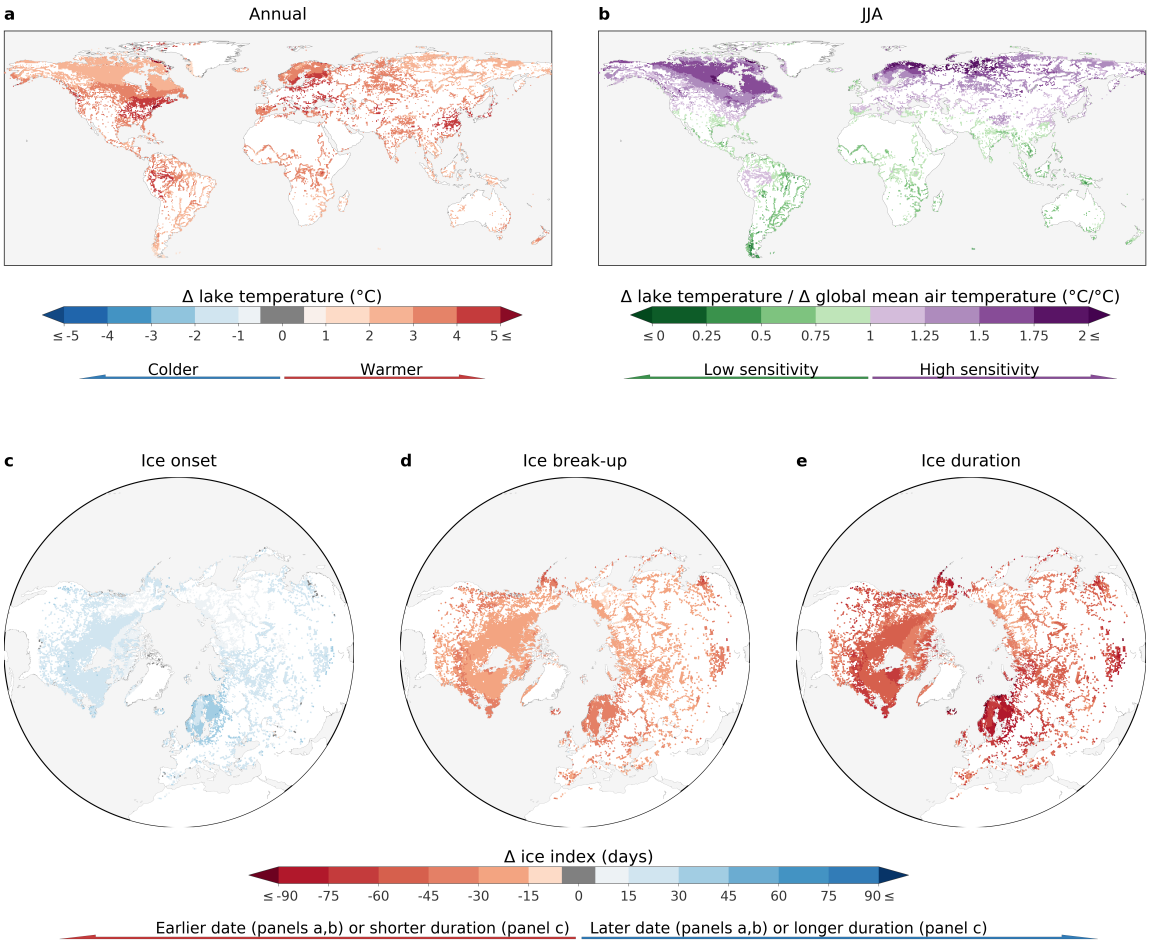

Figure 3: **End-of-century change in lake temperature and ice onset, break-up and duration according to RCP 8.5. a**, Multi-model mean change in annual lake temperatures for **Y projections with X lake models** at 2 m depth. **b**, the mean June-July-August lake temperature change at 2 m depth divided by the change in same-year global mean surface air temperature. **c**, **d** **e**, changes in ice onset, break-up and duration, respectively. All results compare end-of-century (2070-2099) to present-day (1971-2000) conditions.

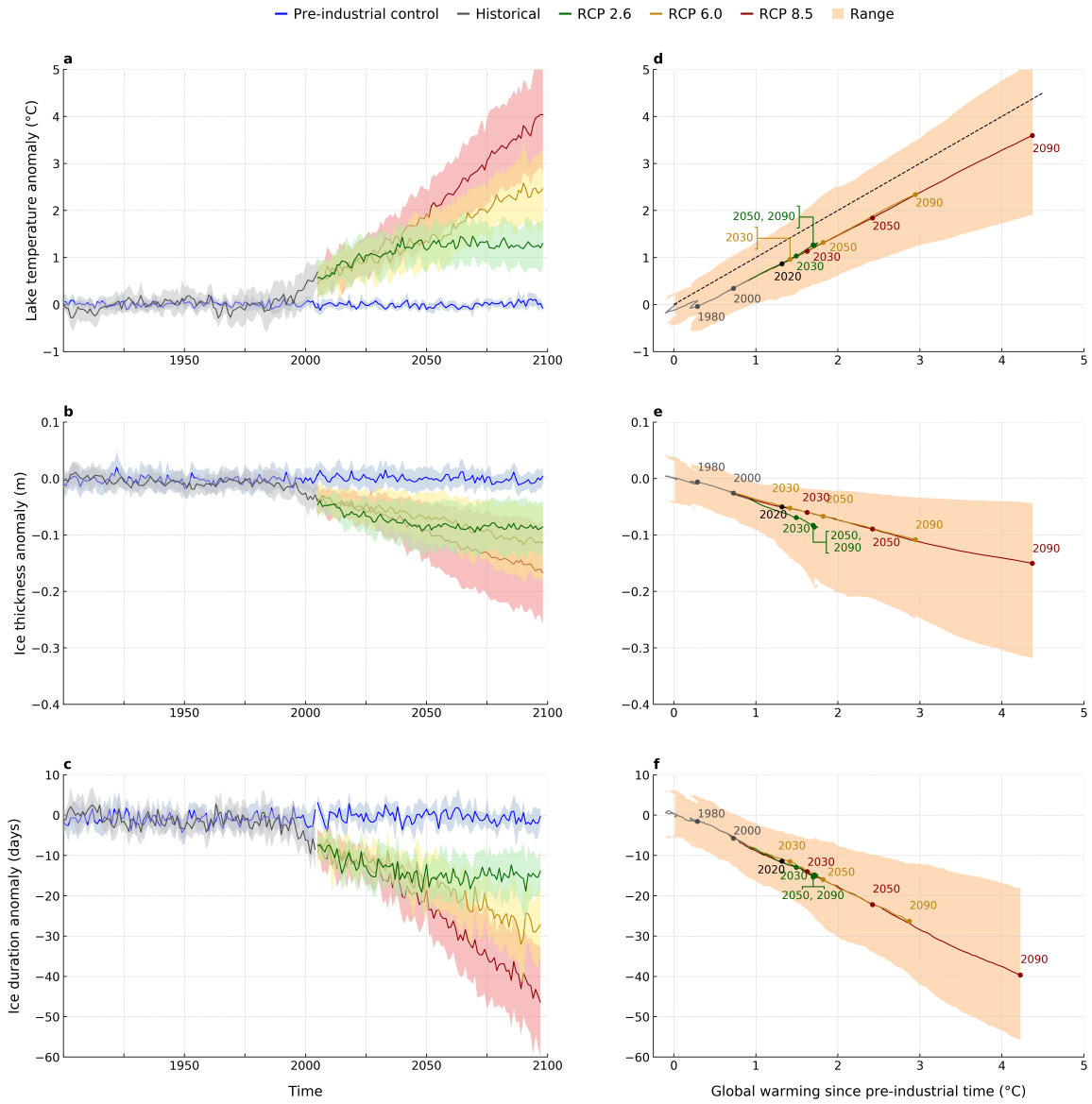

Figure 4: **Anomalies for lake temperature, ice thickness and ice cover. a**, Multi-model mean anomaly time series of annual lake temperatures, **b**, ice thickness and **c**, ice cover duration. Uncertainty bands in panels **a**, **b** and **c** represent +/- 1 standard deviation in lake model ensemble projections. In panels **d**, **e** and **f** the same lake variable anomalies are scaled against surface air temperature anomalies, with uncertainty bands representing the full range of scaled projections.